

Nanocomposite ZnO–SnO₂ Nanofibers Synthesized by Electrospinning Method

Kandasami Asokan · Jae Young Park ·
Sun-Woo Choi · Sang Sub Kim

Received: 9 November 2009 / Accepted: 28 January 2010 / Published online: 9 February 2010
© The Author(s) 2010. This article is published with open access at Springerlink.com

Abstract We report the characterization of mixed oxides nanocomposite nanofibers of $(1 - x)$ ZnO- (x) SnO₂ ($x \leq 0.45$) synthesized by electrospinning technique. The diameter of calcined nanofibers depends on Sn content. Other phases like SnO, ZnSnO₃, and Zn₂SnO₄ were absent. Photoluminescence studies show that there is a change in the blue/violet luminescence confirming the presence of Sn in Zn-rich composition. Present study shows that the crystalline nanocomposite nanofibers with stoichiometry of $(1 - x)$ ZnO- (x) SnO₂ ($x \leq 0.45$) stabilize after the calcination and possess some morphological and optical properties that strongly depend on Sn content.

Keywords Nanofibers · Electrospinning method · Coupled oxide · ZnO · SnO₂

Introduction

Recently, there has been growing interest in one-dimensional nanomaterials such as nanorods, nanowires, nanofibers, and nanotubes of various oxide materials, because of their fundamental scientific interest and also their potential applications in a variety of functional devices [1–4]. Among many one-dimensional nano-structured metal oxides, TiO₂, ZnO, and SnO₂ have been demonstrated to be excellent candidates for ultrasensitive and highly miniaturized

chemical sensors because of their high surface-to-volume ratios and special physical and chemical properties [4–7]. Gas sensing property of semiconductor gas sensors is based on the conductivity (or resistance) change of the materials due to the interaction with the gases to be detected. A nano-structured oxide is particularly useful for fabricating gas sensors because its conductivity can be controlled by the chemi-adsorbed species on its surface. It has been demonstrated to be a highly sensitive material for the detection of many toxic gases. The detection of toxic gases by a semiconductor sensor is extremely important for human and environmental protection. Hence, research on the gas sensors aims at obtaining new sensing materials to achieve highly sensitive and selective devices. However, several problems exist with these single component oxides due to their similar sensitivity to different gases. These sensors have poor long-term stability and need high operating temperatures [5, 8]. It is also observed that the micro-structural change over time leads to reduced sensitivity. Similar problems were observed in other oxides when used for solar cells and catalysts applications [5, 6]. All these results show that oxide sensor characteristics like response, recovery, reproducibility, stability, and linearity vary considerably, and no single oxide sensor provides the desired characteristics.

To overcome these limitations, one approach is to synthesize these sensors by coupling different oxide semiconductors. In such couplings, SnO₂ and TiO₂ or ZnO and SnO₂ received special interests [9–12]. These coupled oxide semiconductors possess characteristics of both the component oxides and allow the possibility of tuning their materials properties as per the requirement for novel applications [11, 12]. A better understanding of such coupled oxides is important in tailoring the properties of next-generation chemical sensors.

K. Asokan
Inter-University Accelerator Centre, Aruna Asaf Ali Marg,
New Delhi 110067, India

K. Asokan · J. Y. Park · S.-W. Choi · S. S. Kim (✉)
School of Materials Science and Engineering, Inha University,
Incheon 402-751, Republic of Korea
e-mail: sangsub@inha.ac.kr

ZnO and SnO₂ belong to wide direct band gap semiconductors, and their E_g band gaps are, respectively, 3.4 and 3.6 eV [11, 12]. Difference in their band gap widths is also found to be very effective way to slow the recombination of electron–hole pairs. Such property consequently increases photocatalytic activity in solar cell applications [10, 11, 13]. This attracted considerable interest, and many investigators exploited various synthesis methods to couple and to obtain nanocomposites of ZnO and SnO₂ including ball milling, microemulsion, partial solid state reduction, and co-precipitation [14–17]. Kunag et al. used ZnO–SnO₂ as core–shell heterojunctions and investigated their properties [13]. Each preparation method and nanomaterial form has unique advantages and disadvantages depending upon the requirement of applications. Recently, there were some interesting investigations employing mesoporous ZnO–SnO₂ nanofibers as ethanol sensors [12]. However, detailed literature survey reflects that there has been no systematic study to understand the morphological and optical properties of these nanocomposite nanofibers. Such study will provide better insight into their possible technological applications.

Present work focuses on the synthesis of nanocomposite nanofibers of mixed oxides containing ZnO and SnO₂ using electrospinning method. These nanofibers were characterized by field emission scanning electron microscopy (FE-SEM), X-ray diffraction (XRD), transmission electron microscopy (TEM), and photoluminescence (PL) spectroscopy.

Experimental Details

Polyvinyl alcohol (PVA) (practical guaranteed grade, Duxsan Pure Chemicals Corp.) with a molecular weight of ~80,000, zinc acetate (Zn(CH₃COO)₂, 99.99%, Sigma–Aldrich Corp.), and tin chloride dihydrate (SnCl₂·2H₂O, 98%, Sigma–Aldrich Corp.) were used as the precursor materials to synthesize the nominal stoichiometry of (1 – x) ZnO-(x)SnO₂ nanofibers.

The electrospinning solutions were prepared as follows. First of all, 2 g of PVA and 1 g of Zn(CH₃COO)₂ were dissolved in 18 g of deionized water by stirring for 10 h at 65–70°C. Next, various amounts of SnCl₂·2H₂O were added to the solution while stirring for 6 h at 70°C. In this study, we prepared six electrospinning solutions of $x = 0.08, 0.20, 0.29, 0.36, 0.45$, and 0.62 in the nominal (1 – x)ZnO-(x)SnO₂ composition. These solutions were loaded into a glass syringe, equipped with a 21-gauge stainless steel needle. The distance between the tip of the syringe needle and the collector of the Al plate was fixed at 20 cm. The syringe needle was inclined at an angle of 25° to the horizontal. This inclined configuration improves a uniform spreading of nanofibers on substrates. A positive

voltage of 15 kV was applied to the needle while the metal collector was grounded. At the same time, a negative voltage of 10 kV was applied to the metal collector to accelerate the electrospinning process. The feeding rate of the solutions was adjusted at a constant rate of 0.2 ml/h by using a syringe pump. The electrospun nanofibers were distributed uniformly over Si wafers, placed on the metal collector. The as-spun nanofibers were calcined at various temperatures and durations in oxygen atmosphere using a tube-type furnace to obtain required phase and morphology. The content of Sn was varied by assuming the stoichiometry to be (1 – x)ZnO-(x)SnO₂. The electrospinning process used in this study is well described in our previous reports [18, 19].

Thermogravimetric-differential thermal analysis (TG-DTA, STA 409 PC, Netzsch) was used to determine the calcination temperature required to remove water and other decomposable organic contents in as-spun nanofibers as well as to decompose the precursors into their corresponding oxide phases. The crystalline structure including the phase purity and morphological features of the synthesized nanofibers were examined using XRD (X'pert MPD PRO, Philips), FE-SEM (S-4300SE, Hitachi), and TEM (JEM2100F, JEOL). The distribution of chemical species was investigated using energy dispersive X-ray spectroscopy (EDS) inbuilt with the TEM. PL (SPEX 1403, SPEX) spectra were measured to understand the substitution effect of Sn in their optical properties.

Results and Discussion

The morphologies of the as-spun (1 – x)ZnO-(x)SnO₂ nanofibers spread on Si substrates were studied using FE-SEM. Figure 1a shows their typical FE-SEM image. TG-DTA was carried out to determine a suitable calcination temperature of as-spun nanofibers. The TG curve of Fig. 1b shows a weight loss. In the range of <200°C, water in the as-spun nanofibers evaporates. Between 200 and 575°C, the organics belonged to PVA, CH₃COO group of zinc acetate and some volatile tin species such as chloride composites evaporate. The DTA curve of the as-spun nanofibers reveals that semiconductor characteristics are present only after annealing at temperatures above 575°C, because below this temperature, both solvent and organic molecule residues can act as obstacles for charge carrier accumulation and transportation in the conduction band. The phase transformation from amorphous (i.e., as-spun nanofibers) to crystalline states (calcined nanofibers) also occurs at this temperature. It should be noted that there was no change in weight loss above 575°C, revealing that a calcination temperature of >575°C is needed to remove the

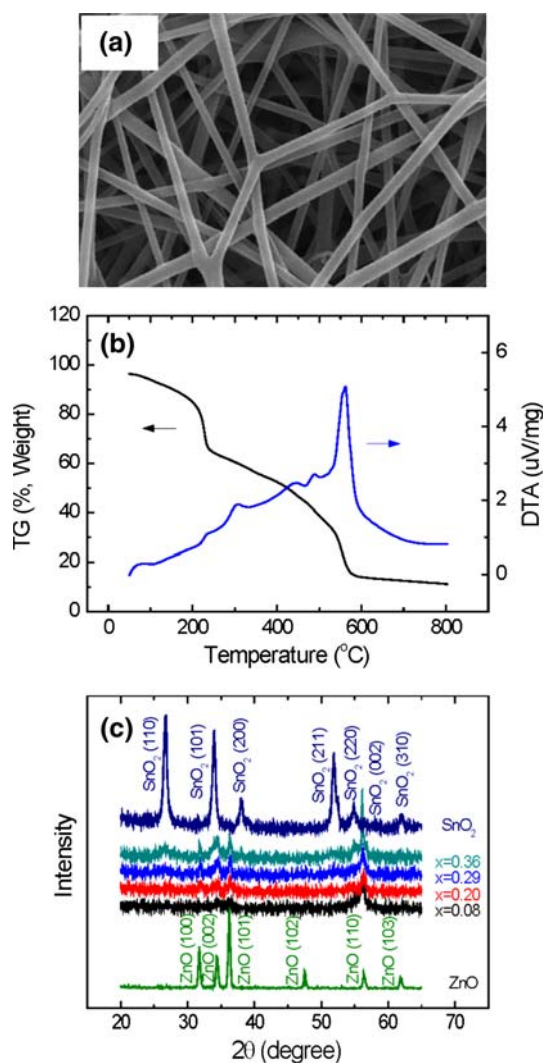


Fig. 1 **a** A typical FE-SEM image of as-spun nanofibers synthesized by electrospinning method. **b** Thermal profiles obtained from TG-DTA for the as-spun nanofibers of $x = 0.45$. **c** XRD patterns of $(1 - x)\text{ZnO}-(x)\text{SnO}_2$ nanofibers calcined at 600°C for 6 h in O_2 ambient

solvent and polymer as well as to fully decompose zinc acetate and tin chloride into a pure ZnO– SnO_2 phase.

In this study, the calcination temperature was optimized to 600°C based on the TG-DTA results. After calcination at 600°C in air for 6 h, well-defined nanofibers get rigid, but their diameter turns thinner due to the decomposition of PVA and the conversion of the metal precursors to the metal oxides. The XRD patterns of calcined nanofibers were analyzed and are shown in Fig. 1c. The composite nanofibers have a polycrystalline nature attributable to various diffraction planes of ZnO and SnO_2 . The XRD profiles exhibit sharp crystalline peaks of high intensity corresponding to the peaks of ZnO and SnO_2 . All diffraction peaks can be perfectly indexed as the tetragonal rutile structure for SnO_2 and a hexagonal wurtzite structure for

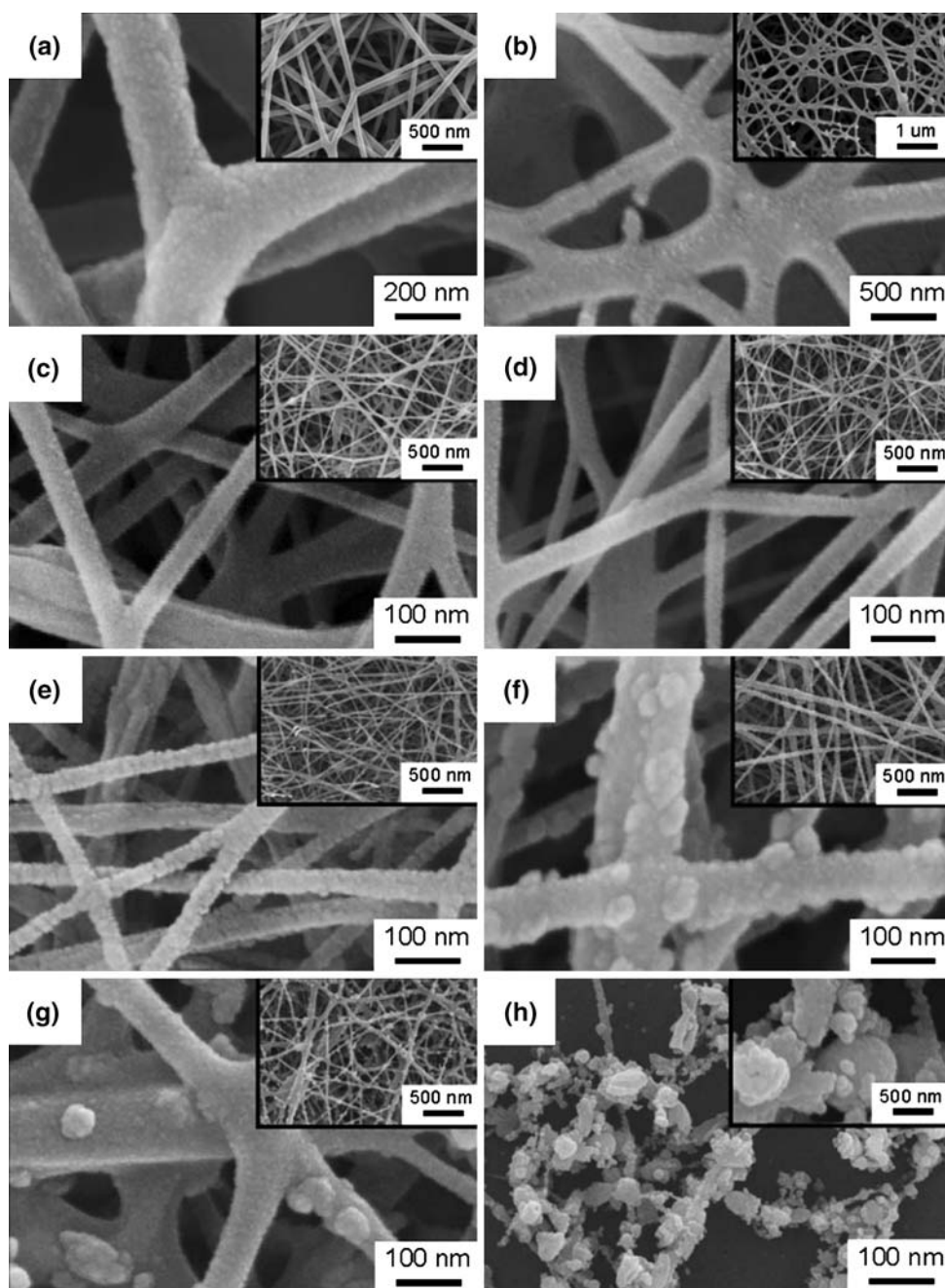
ZnO. No characteristic peaks for impurity, such as SnO , ZnSnO_3 , and Zn_2SnO_4 , were observed [10].

Figure 2 displays the morphological evolution, observed by FE-SEM, of nanocomposite $(1 - x)\text{ZnO}-(x)\text{SnO}_2$ nanofibers, before and after calcination at 600°C in O_2 ambient for 6 h, for various Sn concentrations. Figure 2a and 2b show the typical morphologies of as-spun nanofibers of $x = 0.08$ and 0.45, respectively. The other figures show the calcined nanofibers. Diameters of each composition were measured from the FE-SEM images and are plotted in Fig. 3. As evident, the diameter of the nanofibers depends on the concentration of Sn. According to the results of FE-SEM, nanofibers are formed up to the composition of $x = 0.45$, and above this level, they become Sn-rich nanocomposite clusters and no longer nanofibers. This may be due to the change in the critical limit of processing parameters like viscosity, voltage, and concentration of the electrospinning solutions with increased Sn contents. As mentioned in the experimental part, we kept all the processing parameters constant except the Sn content. More studies by varying the processing parameters of the electrospinning method may help us to understand the reason for the Sn cluster formation.

The TEM image of $(1 - x)\text{ZnO}-(x)\text{SnO}_2$ ($x = 0.36$) nanofibers is shown in Fig. 4. The inset shows a selected area electron diffraction pattern, indicating a polycrystalline nature of the nanofibers. The EDS elemental mapping of the same nanofiber region, indicating spatial distribution of O (blue), Sn (green), and Zn (red), respectively, is shown in Fig. 3b–d. Similar behavior has been observed for all other compositions up to $x = 0.45$, and it is not shown here to avoid repetition.

Figure 5 shows the PL spectra of $(1 - x)\text{ZnO}-(x)\text{SnO}_2$ nanofibers synthesized on Si substrates for various Sn compositions. The PL spectrum of ZnO nanofibers (i.e., $x = 0$) shows a sharp, narrow ultraviolet (UV) band at 370 nm and a broad band centered at around 600 nm. Coupling SnO_2 causes a significant effect on the PL intensities of these nanofibers. The PL spectra for other compositions show a broad spectra and major peak at around 575 nm. A strong UV band edge peak is responsible for the recombination of the free excitons of ZnO. Generally, nanocrystalline ZnO exhibits two peaks in the PL spectrum around 380 and 500 nm. In the present case, the UV emission is observed at a different wavelength compared with most of the reported values for ZnO nanostructures [20]. This may be due to difference in the dimensionality and diameter of the ZnO nanofibers. Another small intensity peak at 468 nm in these ZnO– SnO_2 nanofibers is related to the defect structure of the materials. Chakrabarti et al. also observed two peaks in the visible region at 470 and 510 nm in ZnO nanoparticles [20–22]. The cause of a UV band emission in ZnO is more or less

Fig. 2 FE-SEM images of as-spun nanofibers: **a** $x = 0.08$ and **b** 0.45. FE-SEM images of $(1-x)\text{ZnO}-(x)\text{SnO}_2$ nanofibers calcined at 600°C in O_2 ambient for 6 h: **c** $x = 0.08$, **d** 0.20 **e** 0.29, **f** 0.36, **g** 0.45, and **h** 0.6. The nanofibers are formed up to the composition of $x = 0.45$, and above this critical level, they become Sn-rich clusters and no longer nanofibers



well understood. This is due to a near band edge transition of wide band gap of ZnO, namely the recombination of free excitons through an exciton–exciton collisions process [20, 23]. The green emission of 450–600 nm is usually believed to be related to the intrinsic defect structures, in particular oxygen vacancies. The potential difference between ZnO and SnO_2 allows photoelectrons to easily migrate from the ZnO surfaces to the SnO_2 conduction band. This results in a decrease in the radiation combination of photoinduced electrons on the ZnO surfaces, and further weakening the PL signal. The PL intensity is suppressed with Sn

concentration, while overall spectral features remain almost the same.

The crystalline nanograins of ZnO and SnO_2 coexist in the nanocomposites nanofibers. It is not the case where Sn occupies Zn site or vice versa and form mixed nanofibers of $\text{Zn}(\text{Sn})\text{O}$. The reason for such formation may be related to the synthesis method employed here. The change in (1) polymer solution parameters like molecular weight, solution viscosity, surface tension, solution conductivity, and dielectric effect of solvent, etc., (2) processing conditions namely, voltage, feeding rate, temperature, effect of

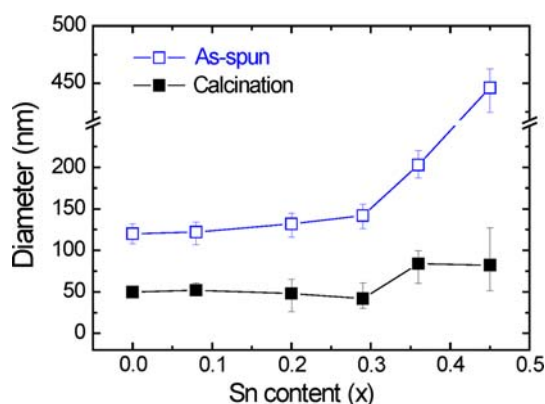


Fig. 3 Variation in the diameter of nanocomposite $(1-x)\text{ZnO}-(x)\text{SnO}_2$ nanofibers as a function of Sn content before and after calcinations

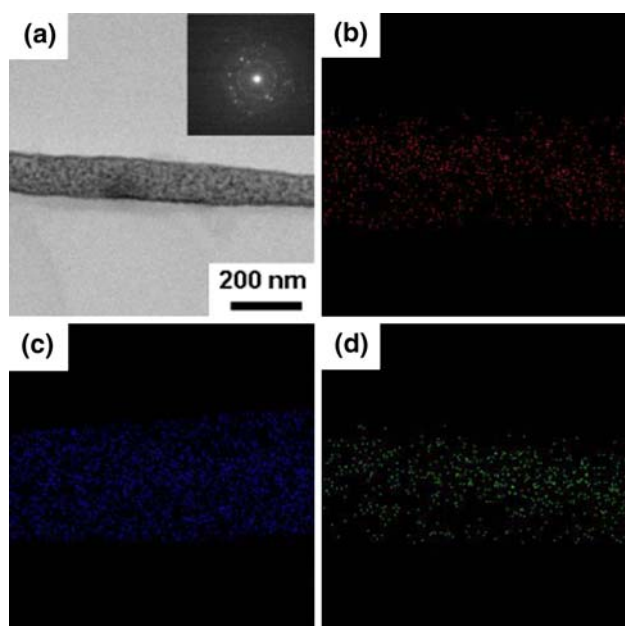


Fig. 4 **a** A typical TEM image of a calcined $(1-x)\text{ZnO}-(x)\text{SnO}_2$ ($x=0.36$) nanofiber. The *inset* shows a selected area electron diffractions pattern, indicating its polycrystalline nature. EDS elemental mapping of the same nanofiber region, showing spatial distribution of **b** Zn (red), **c** O (blue), and **d** Sn (green)

collector, diameter of syringe orifice/needle, and distance between the tip and collector, and (3) ambient parameters including humidity, type of atmosphere, and pressure, etc. has been investigated and found to determine the morphology and properties of the synthesized nanofibers [24]. In our synthesis process, we only varied the concentration of Sn content in the electrospinning solution and kept the other parameters the same. As described above, we used zinc acetate and tin chloride dihydrate, respectively, for Zn and Sn, and these precursors are immiscible. Synthesis temperature was very low in this electrospinning method. This possibly results in the formation of separate ZnO and

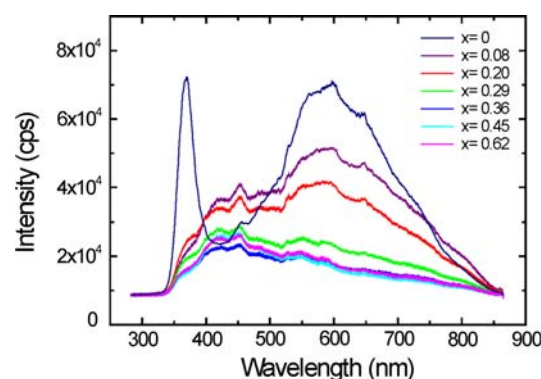


Fig. 5 Typical PL spectra of nanocomposite $(1-x)\text{ZnO}-(x)\text{SnO}_2$ nanofibers calcined at 600°C for 6 h. Coupling SnO_2 shows a significant effect on the PL intensities of pure ZnO nanofibers

SnO_2 nanocomposites of nanofibers up to $x \leq 0.45$. From the electronic structure point of view, these Zn and Sn ions possess different ionic radii and electro-negativities, again implying immiscible nature under normal preparation methods. Thus, these nanocomposites nanofibers are composed of nanograins of SnO_2 and ZnO with crystalline nature.

The nanocomposite nanofibers synthesized in this study possess potential applications in many areas. Applications that have been demonstrated with $\text{ZnO} + \text{SnO}_2$ nanoparticles and thin films, etc. may be extended to these nanocomposite nanofibers [25, 26]. In particular, the nanocomposites of $(1-x)\text{ZnO}-(x)\text{SnO}_2$ ($x < 0.45$) nanofibers are likely to enhance gas sensitivity with better long-term stability, fast response, and recovery time compared with conventional sensors employing simple oxides like SnO_2 , TiO_2 , and ZnO. Their microstructural changes over time will be reduced due the presence of ZnO and SnO_2 nanograins, since both will act in reverse directions [26]. Apart from this, these sensing materials react with selectively with gases unlike gas sensors based on SnO_2 or ZnO alone. This implies that these nanocomposites effectively use the electronic and chemical reactivity of materials for better sensing and photocatalytic applications. Thus, these nanocomposites containing semiconductors like SnO_2 and ZnO are likely to overcome several problems that currently exist with devices fabricated using either just with SnO_2 or ZnO, and the resulting system has the potential for tunable sensitivity and selectivity for many applications [10, 27, 28]. In addition, since these are in the form of nanofibers, it may have advantage in the field of photovoltaic [28]. One of the known ways to increase the conversion efficiency is reducing the radiation losses at the front surface of the solar cell. ZnO has been shown to be plasma resistant and to have 96–97% transmission over the visible spectrum. Photogenerated excess charge carriers can recombine via recombination centers and thus not contribute to the photocurrent. It is a key

feature when describing carrier transport in semiconductors, because it strongly affects the electrical response of the semiconductor at all levels of external excitation.

Conclusions

Present study reported the synthesis and characterization of mixed oxides of $(1-x)\text{ZnO}-(x)\text{SnO}_2$ ($x \leq 0.45$) nanofibers synthesized by electrospinning technique. PVA, $\text{Zn}(\text{CH}_3\text{CO}_2)_2$, and $\text{SnCl}_2 \cdot 2\text{H}_2\text{O}$ were used as the precursor materials to synthesize these nanocomposite nanofibers. The as-spun nanofibers exhibited uniform, smooth fibrous morphology for the compositions of $x \leq 0.45$. Above $x > 0.45$, there was a formation of nanoclusters. The diameters of nanocomposite nanofibers depended on Sn content. The XRD patterns confirmed the presence of ZnO and SnO_2 phases and the absence of SnO, ZnSnO_3 , and Zn_2SnO_4 . The PL measurements showed that there was a change in the blue/violet luminescence confirming the presence of Sn in Zn-rich composition. Above study shows that crystalline $(1-x)\text{ZnO}-(x)\text{SnO}_2$ ($x \leq 0.45$) nanofibers stabilize after calcination and possess morphological and optical properties that strongly depend on Sn content. Some of the potential applications employing these nanocomposites were also discussed.

Acknowledgments This work was supported by a grant from the Fundamental R&D Program for Core Technology of Materials funded by the Ministry of Knowledge Economy, Republic of Korea.

Open Access This article is distributed under the terms of the Creative Commons Attribution Noncommercial License which permits any noncommercial use, distribution, and reproduction in any medium, provided the original author(s) and source are credited.

References

1. G. Yu, A. Cao, C.M. Lieber, *Nat. Nanotech.* **2**, 372 (2007)
2. B. Tian, X. Zheng, T.J. Kempa, Y. Fang, N. Yu, G. Yu, J. Huang, C.M. Lieber, *Nature* **449**, 885 (2007)
3. W. Lu, C.M. Lieber, *Nat. Mater* **6**, 841 (2007)
4. J.A. Rodriguez, M. Fernandez-Garcia, *Synthesis, Properties, and Applications of Oxide Nanomaterials* (Wiley, New Jersey, 2007)
5. M. Batzill, U. Diebold, *Prog. Surf. Sci.* **79**, 47 (2005)
6. J.G. Lu, P. Chang, Z. Fan, *Mater. Sci. Eng. R* **52**, 49 (2006)
7. Z.L. Wang, *J. Phys.: Condens. Matter* **16**, R829 (2004)
8. X.-J. Huang, Y.-K. Choi, *Sens. Actuators B* **122**, 659 (2007)
9. M.M. Oliveira, D.C. Schnitzler, A. J. Zarbin *Chem. Mat.* **15**, 1903 (2003)
10. M. Zhang, T. An, X. Hu, C. Wang, G. Sheng, J. Fu, *Appl. Catal. A* **260**, 215 (2004)
11. A. Alkaya, R. Kaplan, H. Canbolat, S.S. Hegedus, *Renew. Energ.* **34**, 1595 (2009)
12. X. Song, Z. Wang, Y. Liu, C. Wang, L. Li, *Nanotechnology* **20**, 075501 (2009)
13. H. Wang, S. Baek, J. Lee, S. Lim, *Chem. Eng. J.* **146**, 355 (2009)
14. J.H. Yu, G.M. Choi, *Sens. Actuators B* **52**, 251 (1998)
15. Q. Kuang, Z.-Y. Jiang, Z.-X. Xie, S.-C. Lin, Z.-W. Lin, S.Y. Xie, R.-B. Huang, L.-S. Zheng, *J. Am. Chem. Soc.* **127**, 11777 (2005)
16. M. Zhang, G. Sheng, J. Fu, T. An, Z. Wang, X. Hu, *Mater. Lett.* **59**, 3641 (2005)
17. C. Liangyuan, B. Shouli, Z. Guojun, L. Dianqing, C. Aifan, C.C. Liu, *Sens. Actuators B* **134**, 360 (2008)
18. S.-W. Choi, J.Y. Park, S.S. Kim, *Nanotechnology* **20**, 465603 (2009)
19. J.Y. Park, S.S. Kim, *J. Am. Ceram. Soc.* **92**, 1691 (2009)
20. R. Maity, S. Das, M.K. Mitra, K.K. Chattopadhyay, *Physica E* **25**, 605 (2005)
21. B.J. Chen, X.W. Sun, C.X. Xu, B.K. Tay, *Physica E* **21**, 103 (2004)
22. S. Chakrabarti, D. Ganguli, S. Chaudhuri, *J. Phys. D Appl. Phys.* **36**, 146 (2003)
23. J. Bandara, K. Tennkone, P.P.B. Jayatilaka, *Chemosphere* **49**, 439 (2002)
24. S. Ramakrishna, K. Fujihara, W.-E. Teo, T.-C. Lim, Z. Ma, *An Introduction to Electrospinning and Nanofibers* (World Scientific Publishing Company, Singapore, 2005)
25. P.R. Bueno, J.A. Varela, E. Longo, *J. Euro. Ceram. Soc.* **28**, 505 (2008)
26. A. Dodd, A. McKinley, M. Saunders, T. Tsuzuki, *Nanotechnology* **17**, 692 (2006)
27. L. Li, J. Liu, Y. Su, G. Li, X. Chen, X. Qiu, T. Yan, *Nanotechnology* **20**, 155706 (2009)
28. L. Zheng, Y. Zheng, C. Chen, Y. Zhan, X. Lin, Q. Zheng, K. Wei, J. Zhu, *Inorg. Chem.* **48**, 1819 (2009)